International Journal of Biological Macromolecules 181 (2021) 1010–1022

Contents lists available at ScienceDirect

International Journal of Biological Macromolecules

journal homepage: http://www.elsevier.com/locate/ijbiomac

Carboxymethyl cellulose-chitosan composite hydrogel: Modelling and experimental study of the effect of composition on microstructure and swelling response

Kindness A. Uyanga, Walid A. Daoud *

School of Energy and Environment, City University of Hong Kong, Tat Chee Avenue, Kowloon, Hong Kong

ARTICLE INFO

Article history:
Received 20 December 2020
Received in revised form 27 February 2021
Accepted 18 April 2021
Available online 20 April 2021

Keywords:
Flory-Rhener
Clothing insulation (CLO)
Vacuum drying without lyophilization

ABSTRACT

Molecular recognition is essential for the advancement of functional supramolecular natural polymer-based hydrogels. First, a series of carboxymethyl cellulose (CMC)-chitosan (CSN) hydrogels crosslinked with fumaric acid are studied, where the influence of composition on microstructure and swelling is investigated using mathematical modelling and experiment and the hydrolytic properties, microstructure parameters and physicochemical properties are examined. Second, best fit values for the responses are obtained using multiple linear regression and MATLAB R2020a curve fitting and predictive models are generated. Third, the optimum microstructure is loaded with polyethylene glycol (PEG) and bismuth telluride (Bi_2Te_3) and coated on fabric for imparting thermal sensitivity. The results show that (1) optimum microstructure (25.65 ± 1.86 nm mesh size, 116.25 ± 0.00 μmol/cm^3 effective crosslinking-density, 348.03 ± 10.81% swelling, and 62.86 ± 1.11% gel fraction) is found at CMC:CSN = 1:3 for G3; (2) the model shows good agreement with experimental data demonstrating potential for estimating hydrogel swelling and microstructure; and (3) G3/PEG and G3/PEG/Bi_2Te_3 enhance thermal conductivity of fabric at ambient, body, and elevated temperatures. The study demonstrates the potential of the generated model in predicting CMC-CSN swelling and G3 as an ideal host matrix for wearable textiles/devices.

© 2021 Elsevier B.V. All rights reserved.

1. Introduction

Recently, researchers have shown an increasing interest in natural polymer-based hydrogels as matrices for theoretically inexhaustible applications due to their abundance and sustainability compared with depleting petroleum-based synthetic counterparts [1–4]. However, translation from the abounding theoretical models to practical models remains a critical challenge that needs to be addressed. First, translation is dependent on the capacity to develop hydrogels with well-defined microstructure using only green, non-toxic materials and reproducible processes [5] since crosslinking and microstructure control hydrogel properties and performance [6]. Second, an in-depth understanding of hydrogel microstructure – the interplay between components and microstructure formation – promotes translation. Such molecular recognition will provide information on geometrical and interaction pattern of each component necessary for tuning of the components and conditions to obtain desirable hydrolytic properties and microstructure [7]. A method to modify hydrolytic properties, hence, optimize hydrogel microstructure is to vary the hydrogel composition, study in-depth its effect on swelling and microstructure parameters, generate a model to predict the swelling response and microstructure, then test functionability of the optimum hydrogel microstructure as a good host matrix.

Natural polymer-based hydrogels are 3D hydrophilic network structures made up of two or more natural polymers, crosslinker(s) and solvent(s) [8]. Among naturally occurring polymers are cellulose and chitin. Their derivatives carboxymethyl cellulose (CMC) (cellulose derived) and chitosan (CSN) (chitin derived) are widely studied due to their non-toxicity, biocompatibility, extracellular matrix structure, abundance, and cost-effectiveness [9–13]. Moreover, through ionic interaction, they can easily be modified to produce stable and multifunctional composite CMC-CSN structures, having improved properties [9,14,15]. For example, Shang et al. [9] found that CMC-CSN hydrogels exhibit good electromechanical response at different pH, thus are suitable as sensors. Kaihara et al. [14] reported that CMC-CSN blend produces polyion complexes which form stable nanoparticles with semi-interpenetrating network structure. Bao et al. [10] developed smart hydrophilic, temperature-sensitive chiral interfaces for recognition of chiral compounds. Manzoor et al. [16] synthesized stable, highly efficient, and reusable hydrogel beads for metal ions adsorption. Additionally,

* Corresponding author at: B5427, 5/F, Yeung Kin Man Academic Building, City University of Hong Kong, Tat Chee Avenue, Kowloon, Hong Kong.
E-mail address: wdaoud@cityu.edu.hk (W.A. Daoud).

https://doi.org/10.1016/j.ijbiomac.2021.04.117
0141-8130/© 2021 Elsevier B.V. All rights reserved.

Zhang et al. [15] reported that incorporation of CSN to a cellulose framework greatly increases structural integrity, flexibility, and resilience. Ionic crosslinking of CMC with CSN to form CMC~CSN composite is due to inter- and intra-charge compensation between anionic CMC with cationic CSN [4,8,14,17]. CMC alone has a high solubility in water due to the presence of active functional groups such as -hydroxyl (—OH), carboxylic (—COOH), and carbonyl (—C═O) which act as active sites [18]. Thus, ionic crosslinking of CMC with CSN improves CMC matrix density and CSN solubility as —COOH groups are introduced at the glucosamine unit of CSN. Also, CSN is a biodegradable structurally supporting polysaccharide capable of stimulating response [13]. Its active surface can enhance sensing needed for wearable energy textiles. These unique properties make CMC-CSN ideal as matrices for new applications in renewable energy, *e.g.*, loading of energy carriers [19] and thermoelectric materials and anti-microbial energy devices/textiles [8]. Fumaric acid (FU) is a non-toxic, biodegradable, unsaturated dicarboxylic acid, which, when used as crosslinker produces stimuli-responsive CMC-based hydrogels [20]. FU also exhibits antibacterial and anticarcinogenic properties [21] which are dermatologically advantageous. Polyethylene glycol (PEG) is biodegradable, non-toxic, with excellent solid-liquid transformation at a wide temperature [22–24], an electrically insulating and electron-donating amphiphilic water-soluble polymer [25] with low thermal conductivity capable of enhancing thermal insulation. PEG has been combined with CMC-based hydrogels as an effective network modifier to enhance hydrogel properties [26]. Incorporation in a hydrogel matrix can be useful to achieve desired thermal control – hydrogel swelling to absorb heat or hydrogel shrinking to exude bound water which leads to cooling *via* evaporation. These impulse responses can be tapped for the advancement of smart skin-contacting energy devices. Bismuth telluride (Bi_2Te_3) is an excellent thermoelectric material [27–29] with a high thermoelectric figure of merit at ambient (15–25 °C) temperature. For wearable energy textiles, Bi_2Te_3 can enhance the conversion of waste heat dissipated from the human body into electrical power induced by the difference in temperature between the human body and the ambient temperature [30,31]. The dissipated heat can be harvested for powering wearable devices. Therefore, natural polymer-based composite hydrogels synthesized by blending CMC, CSN, FU, Bi_2Te_3 and/or PEG can advance the development of smart thermo-sensitive matrices for wearable energy applications. Herein, CMC-CSN, FU, PEG and Bi_2Te_3 were used as bi-polymer hydrogel backbone, crosslinker and functional components, respectively for the synthesis of the hydrogels.

In our previous work, the effect of different non-cytotoxic crosslinkers, namely, citric acid (CA), fumaric acid (FU), tartaric acid (TA), and zinc ions (Zn^{2+}), on hydrogel microstructure was examined, where CMC-CSN crosslinked with FU (CMC~FU~CSN) shows the optimum microstructure and properties. Enhanced crosslinking is attributed to the reduced amount of hydrophilic functional groups in FU when compared with the other crosslinkers. In this study, the influence of CMC and CSN ratio on swelling and microstructure of CMC~FU~CSN is investigated using a modified method. First, the ratio of CMC and CSN is varied between 1 and 5, and hydrogel equilibrium swelling ratio and microstructure parameters are determined experimentally and according to Flory Rhener's equation. Crosslinking, structure, and stability of the hydrogels are confirmed using Fourier transform infrared spectroscopy (FTIR), differential scanning calorimetry (DSC), X-ray diffraction (XRD), scanning electron microscopy (SEM) and thermographic analysis (TGA). Second, mathematical models to relate the influence of (1) CMC and CSN ratio on equilibrium swelling ratio and (2) swelling ratio on mesh size, molecular weight between crosslinks and effective crosslinking density for the CMC ~ FU ~ CSN composite hydrogels are developed and validated. Third, the optimum microstructure is loaded with PEG and Bi_2Te_3, coated on fabric, and the coated fabric is characterized for thermal conductivity, temperature-sensitivity, and clothing insulation (CLO). It is hypothesized that (1) increasing CSN content during hydrogel synthesis will improve the microstructure and crosslinking density since CSN introduces more amide groups into the hydrogel system, which interacts with the COO^- of CMC through ionic interaction to suppress swelling, and (2) addition of PEG will enhance temperature-sensitivity of the hydrogel since PEG has a high phase change enthalpy. To the best of our knowledge, this study is the first to experimentally and theoretically demonstrate the tuning of CMC and CSN composition to examine its influence on the swelling and microstructure of CMC~FU~CSN hydrogels. This study is significant because (1) the development of a model that relates CMC:CSN with hydrogel swelling is important for understanding CMC~CSN composite hydrogels, predicting microstructures, and designing CMC~CSN systems with desirable hydrolytic properties; (2) the developed mathematical models will offer predictive capabilities on (a) swelling ratio for varying amounts of CMC and CSN, and (b) microstructure parameters where equilibrium swelling ratio is known or estimated from (a) for CMC~FU~CSN hydrogels; and (3) the G3/PEG and G3/PEG/Bi_2Te_3 hydrogels fabrics developed show potential for the advancement of natural bi-polymer based hydrogels for thermal control for smart wearable energy textiles/devices.

2. Materials and methods

2.1. Materials

Carboxymethyl cellulose sodium (average molecular weight, Mw: 250 kDa, 700 mPas viscosity at 25 °C), polyethylene glycol (Mw: 8000 g/mol) and fumaric acid, 99% were purchased from Alfa Aesar (Heysham, England). Chitosan (Mw: 100 kDa, 5–20 mPas, 0.5% acetic acid at 20 °C) was purchased from Tokyo Chemical Industry Co. Ltd. (Tokyo, Japan). Bismuth telluride powder, 99.99% was purchased from China Materials Technology Co. Ltd. (Jiangxi, China), ethanol, 75% was purchased from Uni-Chem chemical reagents (China) and acetic acid, ≥99% reagent grade from VWR Chemicals BDH® (France, Europe). All chemicals were of analytical grade and were used as purchased without further purification. De-ionized water (18 MΩ cm) was used throughout the experiment.

2.2. Design approach for swelling study

Box-Wilson design was selected [32]. The independent variables CMC and CSN ratios were designated X1 and X2, respectively; and varied between 1 and 5. Crosslinker amount, X3 was kept constant, so its influence on the dependent variable was not considered. The experimental conditions are given (Table S1, Supplementary information). Nineteen hydrogels and non-crosslinked bi-polymer backbone were developed. Ten experiments (G1–G10) were repeated to increase prediction results. Total number of observations was 30.

2.3. Preparation of CMC~FU~CSN composite hydrogels

The hydrogels were prepared by chemical gelation at 25 °C following a similar procedure [8]. Briefly, 1 wt% of CMC, 0.6 wt% of FU and 1 wt% of CSN (in 1 wt% of acetic acid) homogenous solutions were separately prepared. First, 10 mL CMC solution was crosslinked with 10 mL FU solution to form CMC~FU solution. Second, while stirred at 500 rpm, CMC ~ FU was added dropwise into 10 mL CSN solution to form CMC~FU~CSN hydrogel, G1. Using ratios given in Table S1 and repeating the above steps, the other hydrogel solutions (G2–G19) were prepared. Then, the hydrogel solutions were poured into Petri dishes, allowed to stand overnight to remove entrapped gas, and dried in a vacuum oven (48 h at 60 °C) without a lyophilization step. The dried hydrogels were brought out, washed to remove untreated entities, and re-dried for 24 h. The CMC~FU~CSN hydrogels were stored in a desiccator until characterized. Non-crosslinked CMC~CSN (G0) was also prepared as the control sample.

2.4. Characterization of CMC~FU~CSN hydrogels

G1, G2, G3, G4, G5, G6, G7, G8, G9 and G10 were characterized for microstructure and crosslinking by studying their hydrolytic (swelling, water absorbency (%) and gel fraction (%)), thermal, morphological, structural, and chemical properties. Microstructure parameters were also calculated.

Hydrogel hydrolytic properties in de-ionized water (pH 7.2) at 25 °C for 48 h were measured [8]. Swelling was measured gravimetrically within first 7 h and at 48 h. Water absorbency (A_w) was $(W_s - W_d)/W_d$ where W_s is weight of swollen hydrogel and W_d is weight of dry composite hydrogel before incubation. Then, a mass of dried hydrogel was immersed in de-ionized water. The insoluble part was dried and weighed. Gel fraction (G_f) was calculated as (W_i/W_d) where W_i is weight of dried insoluble part, and W_d is weight of dried matrix before immersion in water.

The functional groups and chemical composition of the hydrogels were studied using FTIR spectrometer (IRAffinity-1, Shimadzu, Japan). All samples were analyzed as powder, thoroughly mixed with KBr powder, compressed into 1 mm transparent pellet over 4000 to 400 cm^{-1}. The XRD patterns of the hydrogel matrices at $5° \le 2\theta \le 60°$ were obtained using a PANalytical X'Pert^3 Powder (PANalytical, Netherlands) equipped with a CuKα radiation source, operated at 40 kV and 40 mA. The hydrogels were gold-sputtered and surface micrographs investigated using ZEISS EVO MA10 SEM (Carl Zeiss Microscopy, USA), operated at an accelerating voltage of 10 kV. DSC-TGA was conducted using the Mettler Toledo Thermographic and Differential Scanning Calorimetry (TGA/DSC) 1 (Mettler Toledo, Switzerland). The hydrogels were heated at 10 °C/min at 25–400 °C under a nitrogen flowrate of 50 mL/min.

Least square multiple regression analysis was used to analyze the relationship between the independent variables (CMC ratio and CSN ratio) and the dependent variable (equilibrium swelling ratio). Based on experimental swelling data, the multiple linear regression equation was used to fit the polynomial equation:

$$\hat{Y} = \beta_0 + \sum_{i=1}^{n} \beta_i X_i + \sum_{i=1}^{n} \beta_{ii} X_i^2 + \sum_{i=1}^{n-1} \sum_{j=2}^{n} \beta_{ij} \beta_{12} X_i X_j$$

where $\hat{Y}$—predicted swelling response, β_0—model intercept, β_i —linear coefficient, β_{ii}—quadratic coefficients β_{ij}—model interaction coefficients, X_i, X_j are coded values for variables i and j, and n—total number of variables. The analyses were conducted using Excel and MATLAB R2020a. Lack of fit of the model was evaluated at confidence level equals 95%. The predicted model was validated by considering the overall regression accuracy, the significance of F (*i.e.,* overall P), individual p-values of the coefficients, residuals, and experimental method. In the experimental method, five new hydrogels (H1-H5) were synthesized at CMC:CSN = 1.5:1, 1:1.5, 3.5:1, 1:3.5, and 3.5:2 and equilibrium swelling ratio measured and compared with predicted values.

2.5. Evaluation of microstructure parameters

Average molecular weights between crosslinks ($\overline{M}_C$) was measured using Eq. (1) [33].

$$\frac{1}{\overline{M}_C} = \frac{2}{\overline{M}_N} - \frac{\overline{v}\left[\ \ln(1-V_N) + V_N + XV_N^{\,2}\ \right]}{V_S\left(V_N^{\frac{1}{3}} - \left(\frac{V_N}{2}\right)\right)} \quad (1)$$

where volume fraction of swollen polymer network, $V_N = \left(\frac{1}{1+(S_R-1)\frac{\rho_N}{\rho_S}}\right)$; $\overline{M}_N$ –molecular weight of primary polymer chains; $\overline{v}$ –specific volume of polymer network; Flory-Huggins solvent-polymer interaction parameter, X=0.463; solvent molar volume, V_S=18 cm^3/mol; S_R – equilibrium swelling ratio; ρ_N –mass density of polymer network; and solvent mass density, ρ_S=0.99707 g/cm^3. Hydrogel density was calculated from hydrogel dry mass and change in hexane volume after dipping in hexane. Effective crosslinking density, $V_C = \left(\frac{\rho_N}{M_C}\right)$ and mesh size (nm) = $0.1748 \times (M_C{}^{1/2}) \times (S_R{}^{1/3})$ [18].

2.6. Preparation and characterization of G3/PEG and G3/PEG/Bi_2Te_3 coated textiles

First, 0.03 mol/L PEG solution was prepared. 10 mL PEG solution was added into 50 mL G3 hydrogel solution and stirred at 400 rpm, 25 °C for 30 min to form G3/PEG solution. G3/PEG was reproduced, and 10 mL Bi_2Te_3 solution was added to form G3/PEG/Bi_2Te_3. The Bi_2Te_3 solution was prepared by dissolving 0.1 g Bi_2Te_3 in 100 mL ethanol. Second, the prepared formulations were applied on scoured fabric using a dip-pad method as follows. Interlock knitted cotton fabric was washed using 2 g/L non-ionic detergent (for 30 min at 400 rpm) and dried at 80 °C. The scoured fabric was cut into 2 cm × 2 cm, and 5 cm × 5 cm pieces; and were separately dipped into G3/PEG and G3/PEG/Bi_2Te_3 formulations for 10 min. Padding was carried out using a laboratory padder set at 0.65 MPa and 7.5 rpm to get a wet pick up of 100%. The coated fabrics were dried at 80 °C and cured at 120 °C for 3 min after which they were washed with de-ionized water, re-dried at 80 °C, and stored in the desiccator until characterization. Also, scoured untreated cotton samples were selected and labelled as uncoated samples. Third, the coated and uncoated samples were characterized for thermal sensitivity at ambient temperature (T = 15 °C), on human skin (33.2 °C), and at 45 °C. The thermal sensitivity analysis was conducted as follows. At ambient temperature, the fabrics (4 cm × 4 cm) on a glass Petri dish (14.5 cm × 1.4 cm × 14.5 cm) were placed on a 15 °C ice bath. A plastic wrap was placed between the ice bath and the Petri dish to avoid water absorption. On human skin, the fabrics were cut into 2 cm × 4 cm and simultaneously placed on the surface of the arm at 33.2 °C. At elevated temperature, 4 cm × 4 cm fabrics on the glass Petri dish were placed on a hotplate set at 45 °C. For the three temperature conditions, the fabrics were first allowed to attain steady condition for 15 min, then examined for 20–30 min. Thermal images were acquired using FLIR 53–24° (FLIR Systems Inc., USA) and analyzed using the FLIR Tools software (Version 6.4). Further, thermal resistivity and cloth insulation properties were estimated. Fabric thermal resistivity, R ((m^2K)/W) was calculated as ratio of fabric thickness, L (m) to fabric thermal conductivity, k (W/mK). Thermal conductivity was measured using C-Therm (C-Therm Technologies, Fredericton, Canada). An average of 3 readings was obtained. The clothing insulation (CLO) value was estimated using the thermal resistance whereby 1 CLO = 0.155 (m^2K)/W.

3. Results and discussion

3.1. Preparation of CMC~FU~CSN hydrogels

The proposed reaction mechanism for G0 and the developed hydrogels (Fig. 1) are as follows. Anionic polyelectrolyte carboxymethyl cellulose sodium reacts with cationic polyelectrolyte chitosan by ionic crosslinking to form G0 (CMC~CSN) [4,17]. Furthermore, at the introduction of FU, crosslinking mechanism of G0 in the presence of FU is esterification. The —COO^- and —OH groups of FU crosslink through ester formation leading to the development of the hydrogel.

3.2. Hydrolytic properties

The hydrogels show moderate and super swelling (Fig. 2a) in de-ionized water (pH 7.2). G1, G3, and G5 show moderate swelling <2000% and water absorbency <1000% (Fig. 2b) while G2, G6, G7, G9, and G10 show increasing super-absorbency. G5 shows the lowest water absorbency (Fig. 2b), yet the lowest gel fraction (Fig. 2c). The swelling and water absorbency results corroborate. First, Fig. 2 shows that G1, G3, G7 and G9 show swelling (541.46 ± 7.89%, 348.03 ± 10.81%, 2549.70 ± 17.12%, and 3169.20 ± 20.00%), water absorbency (534.71 ± 8.57%, 397.96 ± 11.24%, 1570.78 ± 22.78% and 2942.00 ± 27.23%)

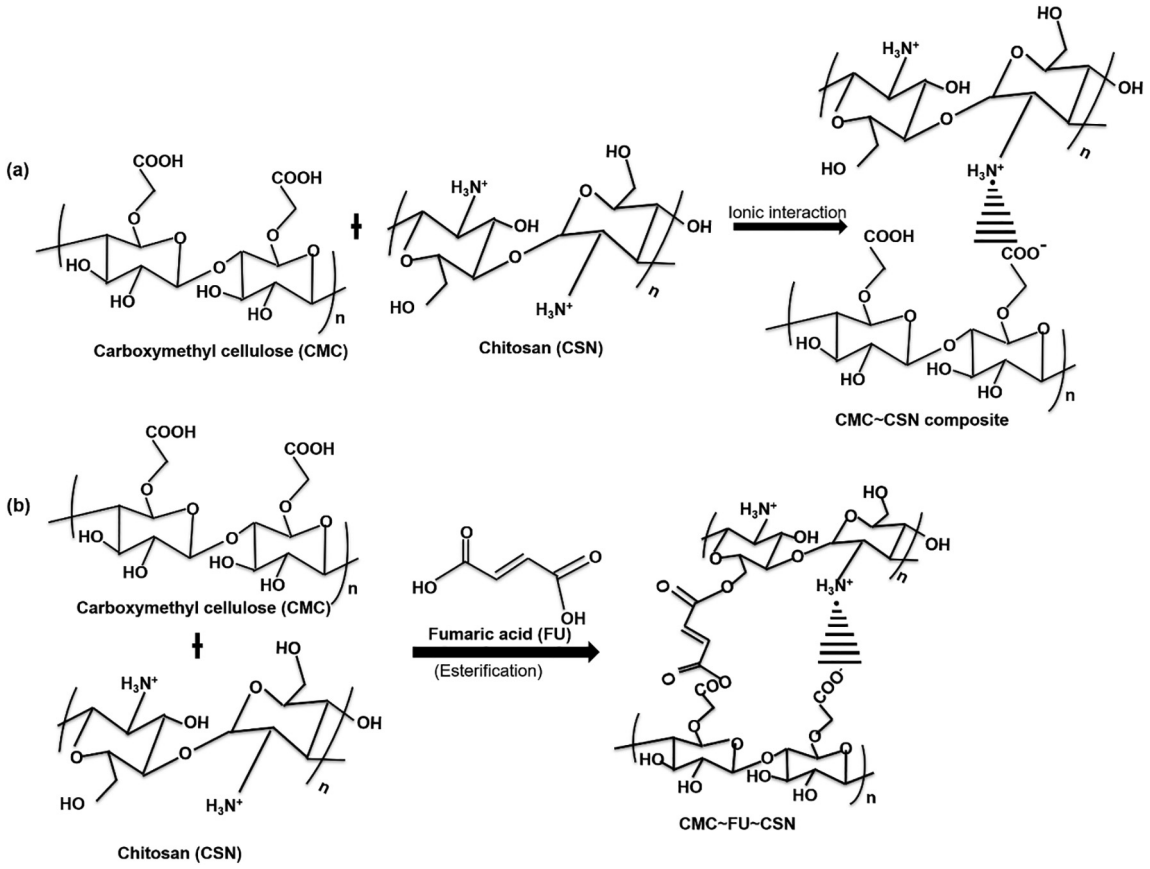


Fig. 1. Proposed reaction mechanism for the formation of (a) CMC~CSN and (b) the CMC~FU~CSN hydrogels.

and enhanced hydrolytic stability (60.74 ± 0.42%, 62.86 ± 1.11%, 68.31 ± 1.81% and 68.80 ± 0.27%) when compared with G0 (428.96 ± 5.86% swelling, 377.02 ± 10.21% water absorbency, and 54.44 ± 0.24% gel fraction). This could be due to improved crosslinking following ionic interaction and esterification, unlike for G0 where crosslinking is mainly by ionic crosslinking [8,20,34]. The enhanced hydrolytic properties of G1 and G3 could be attributed to enhanced crosslinking due to FU while that of G7 and G9 could be due to electrostatic interaction between CMC and CSN at higher polymer content [35]. Super-absorbency of G7 and G9 with high gel fraction is attributable to the increased amount of CMC and CSN since the more balanced the charge stoichiometry and polyions content, the higher the degree of ionic crosslinking and microstructure stability. Second, water uptake is seen to be directly proportional to CMC amount (which introduces more COOH and OH) but inversely proportional to CSN amount (which creates more balance between ionic crosslinks and NH2 groups). CMC enhances electrostatic charges which double swelling. Swelling decreases with the increasing balance between ionic crosslinks, increasing NH2 content in the backbone. The presented results agree with that reported in the first paper in this series, and with other previous studies on CMC~CSN [35–37]. For example, Wang et al. reported 306 ± 8% swelling for CMC~CSN [37].

Thus, (1) G1 and G3 exhibit improved microstructure and crosslinking density; and (2) the higher the compositional content of CMC (*i.e.,* more OH^- and COO^- from CMC and fewer amine groups from CSN), the higher the water uptake and lower the crosslinking density and hydrogel microstructure.

3.3. Microstructure parameters

Table 1 shows that M_C varied between 9376 ± 12 g/mol and 108,033 ± 48 g/mol, mesh size between 25.65 ± 1.86 nm and 198.88 ± 5.76 nm, while V_C between 9.09 ± 0.00 μmol/cm^3 and 116.25 ± 0.00 μmol/cm^3. The equilibrium swelling ratio is directly proportional to M_C and mesh size but inversely proportional to V_C. G3 has a very high crosslinking density when compared with the other hydrogels. The low swelling ratio of G3 could be the reason for the observed significant enhancement in V_C. Quantitatively, a low swelling ratio translates to (1) a very high volume fraction of polymer network (V_N) (Eqs. (1) and (2)) a significantly low average molecular weight between crosslinks (M_C). G3 has V_N about 5.86 times that of the most swelling hydrogel, G10 and M_C about 0.09 times that of G10. With such least M_C value and mass density (ρ_N) within the same range as that of the other hydrogels, effective crosslinking density, V_C ($=\rho_N/M_C$) significantly increases for G3. Arranged according to decreasing V_C, G3 > G1 > G5 > G4 > G10 > G7 > G9 > G2 > G8 > G6. Hence, this result corroborates the hydrolytic properties results for the non-superabsorbent class of hydrogels that G3 has optimum microstructure. For the superabsorbent hydrogels, Table 1 confirms that the observed enhancement in gel fraction could primarily be due to ionic interaction of CMC and CSN at the varied amounts and not an effect of crosslinking with FU.

3.4. Chemical and structural properties

FTIR, DSC and XRD analyses were used to confirm crosslinking of the hydrogels. The FTIR and XRD peaks were analyzed using SpectraGryph software v1.2.13 with peak label function set at 5% threshold.

The FTIR spectra (Fig. 3a and b) show the chemical features of CMC, CSN, CMC~CSN (G0), FU and the crosslinked hydrogels (SpectraGryp prominence = 4). CMC shows characteristic absorption peaks at 3600–3200 cm^{-1}, 2915 cm^{-1}, 1598 cm^{-1}, and 1060 cm^{-1} corresponding to —OH bending, —CH stretching, —COOH group, and —CO stretching vibrations [38–40], while CSN shows bands at 3600–3250 cm^{-1}, 2929 cm^{-1}, 1655 cm^{-1}, and 1063 cm^{-1} ascribable to stacking of —OH and —NH stretching vibrations, —CH_2 group, amide group,

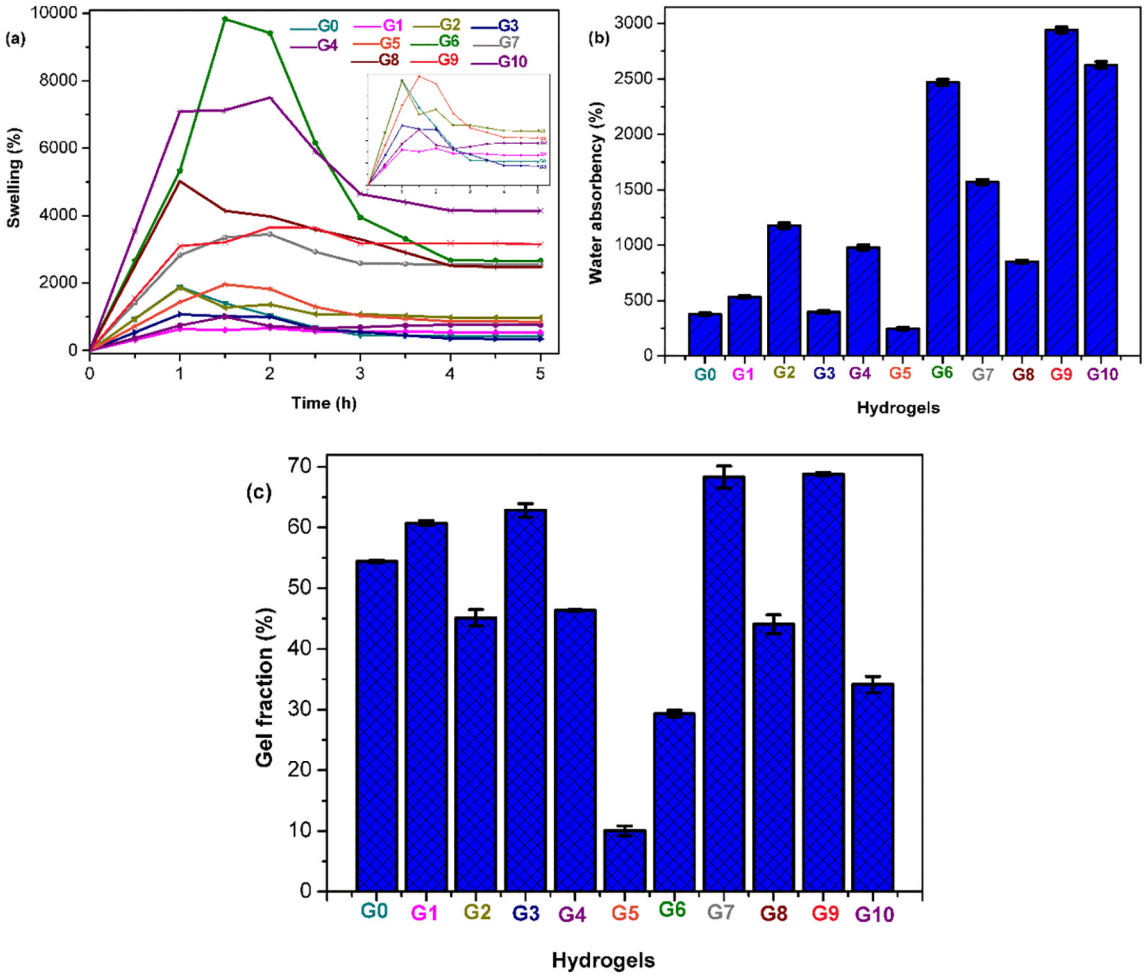


Fig. 2. Hydrolytic properties (a) swelling (%) within 5 h, (b) water absorbency (%) after 48 h and (c) gel fraction after 48 h immersion in water of the hydrogels.

ether of saccharide ring (C—O), respectively [38]. FU shows prominent peaks at 3084 cm^{-1}, 1699 cm^{-1}, 1276 cm^{-1}, 896 cm^{-1}, and 645 cm^{-1} ascribable to C═C—H stretching, C═O stretching vibration, —CO vibration, OH stretching, and deformation vibration of O═C—O, respectively. G0 exhibits absorption bands from CMC and CSN. The appearance and prominence of the peak at 1077 cm^{-1} could be due to ionic interaction between $—COO^-$ group of CMC and NH_3^+ group of CSN [39]. All the crosslinked composite hydrogels show mixed characteristic bands of G0 and FU and corresponding absorption and vibration bands like G1 with differences in their intensity and positions. For example, the COOH bands at 1699 cm^{-1} in pure FU shifted to lower wavenumbers ranging between 1508 cm^{-1} and 1561 cm^{-1}. Similarly, the O═C—O group of FU at 645 cm^{-1} is shifted to either higher or lower wavenumber with reduced peak intensities in the crosslinked hydrogels. Again, the intensity and sharpness of the COOH bands at 1415 cm^{-1} are almost disappeared for the crosslinked hydrogels. These are ascribable to interactions during crosslinking and hydrogen bonding [40]. The presented results are like those published [8,40].

The XRD patterns (Fig. 4a and b) show a typical sharp peak for CMC at $2\theta = 20.03°$ and two characteristic CSN peaks at $2\theta = 9.79°$ and 20.01° indicating their amorphous nature [8,18]. The CSN peak at $2\theta = 9.79°$ is attributable to crystal form I (amine I (—N—CO—CH_3))

Table 1
Calculated microstructure parameters of CMC~FU~CSN (G1), CMC~FU~2CSN (G2), CMC~FU~3CSN (G3), CMC~FU~4CSN (G4), CMC~FU~5CSN (G5), 2CMC~FU~CSN (G6), 2CMC~FU~3CSN (G7), 2CMC~FU~5CSN (G8), 3CMC~FU~CSN (G9) and 3CMC~FU~2CSN (G10) presented as mean ± SD ($n = 3$).

Hydrogel code	SR	ρ_N (g/cm^3)	Experimental data		
			Mc (g/mol)	Mesh size (nm)	Effective crosslinking density (μmol/cm^3)
G1	5.41 ± 0.06	1.29 ± 0.05	49,572 ± 52	68.32 ± 2.12	26.02 ± 0.00
G2	9.80 ± 0.08	1.04 ± 0.00	94,841 ± 61	115.20 ± 5.14	11.00 ± 0.00
G3	3.48 ± 0.10	1.09 ± 0.05	9376 ± 12	25.65 ± 1.86	116.25 ± 0.00
G4	7.57 ± 0.11	0.83 ± 0.05	73,651 ± 16	93.15 ± 3.16	11.30 ± 0.00
G5	8.58 ± 0.09	1.47 ± 0.05	92,878 ± 10	109.06 ± 11.50	15.80 ± 0.00
G6	26.70 ± 0.15	1.52 ± 0.00	107,801 ± 38	171.54 ± 11.10	14.10 ± 0.00
G7	25.50 ± 0.23	1.46 ± 0.05	107,737 ± 50	168.88 ± 9.86	13.58 ± 0.00
G8	24.89 ± 0.19	0.98 ± 0.05	107,510 ± 51	167.34 ± 4.89	9.09 ± 0.00
G9	31.69 ± 0.12	1.37 ± 0.10	107,915 ± 45	181.71 ± 9.21	12.70 ± 0.00
G10	41.48 ± 0.10	1.52 ± 0.05	108,033 ± 48	198.88 ± 5.76	14.05 ± 0.00

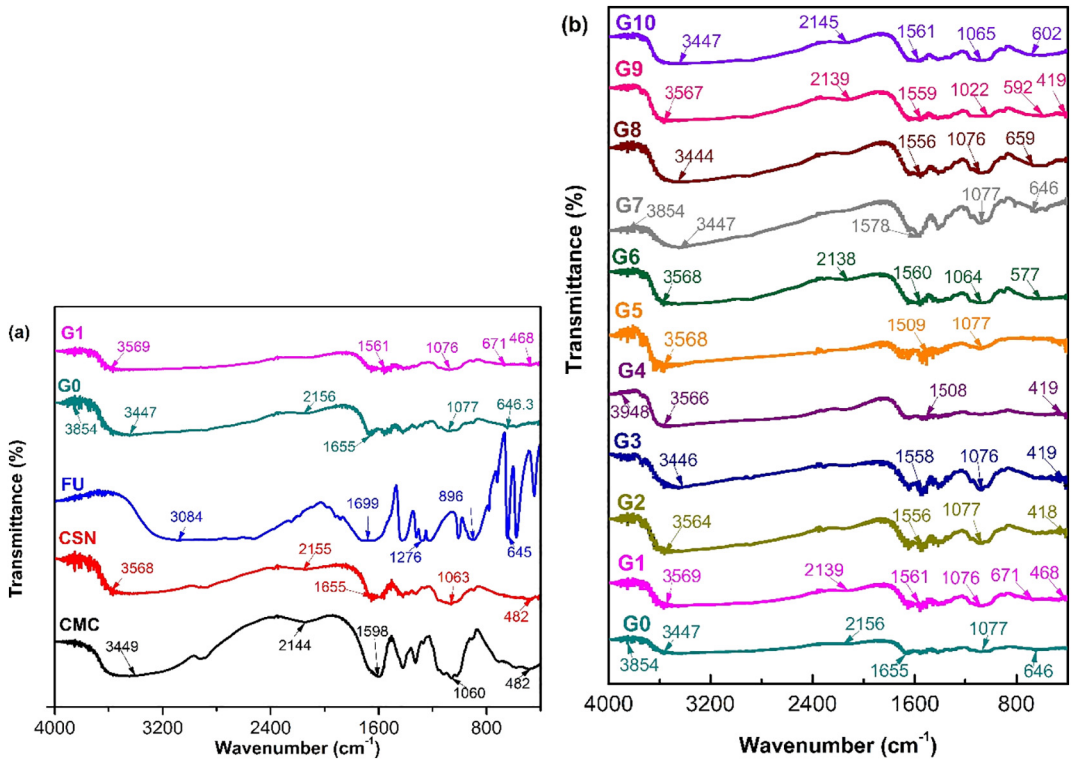


Fig. 3. FTIR spectra of (a) CMC, CSN, FU, G0 and G1 and (b) G0 and the hydrogels.

and that at $2\theta = 20.01°$ ascribable to crystal form II (amine II ($-NH_2$)) and corresponding to crystallographic planes (020) and (110), respectively [41,42]. For G0 and the hydrogels, the CSN peak at $2\theta = 9.79°$ disappears while that at $2\theta = 20.01°$ reduces in intensity due to the amorphization process. It also confirms the electrostatic interaction between CMC and CSN and good compatibility between CMC, CSN and FU

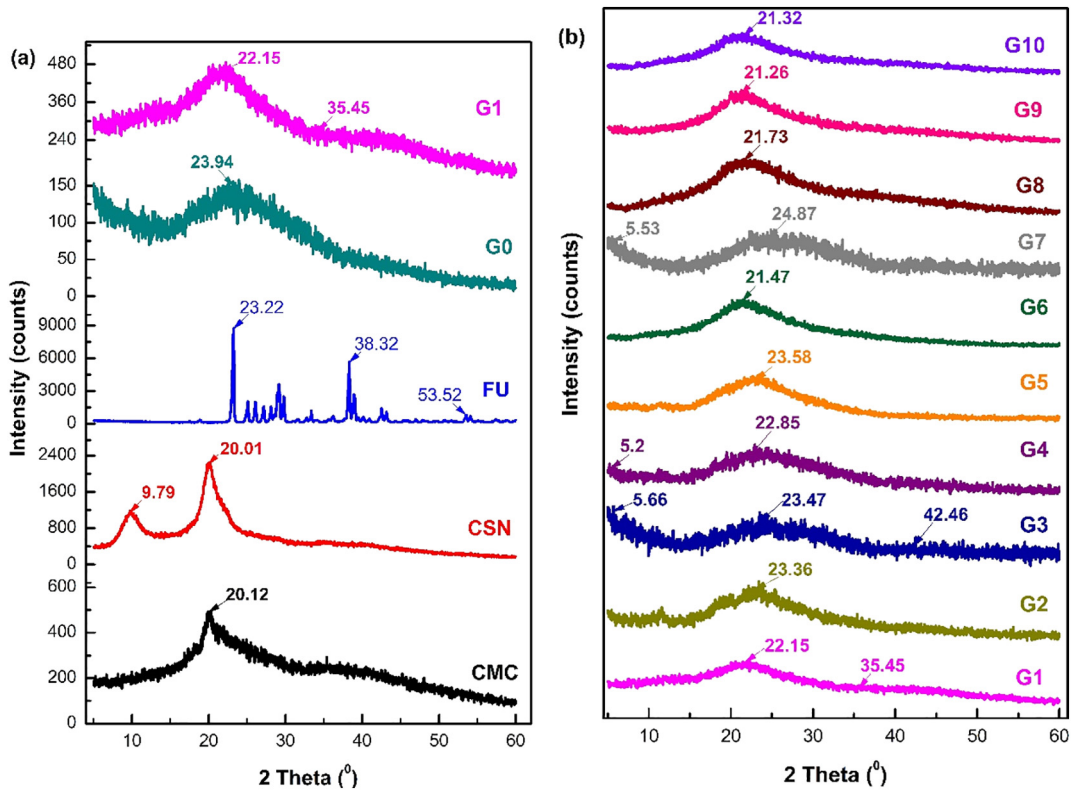


Fig. 4. XRD pattern of (a) CMC, CSN, FU, G0 and G1 showing crosslinking, and (b) the crosslinked hydrogels G1-G10.

in the formation of G0 and the hydrogels. Thus, G0 expresses lower crystallinity, reduced peak intensity and a shift towards $2\theta = 23.94°$ (Fig. 4a). This demonstrates the strong intermolecular interaction between CMC and CSN chains which destroys the crystalline nature of CSN. FU shows six intense peaks at $2\theta = 23.22°$, 29.19°, 33.38°, 38.32°, 42.52° and 53.52° which become significantly reduced or almost disappeared for all the hydrogels confirming intermolecular interaction and crosslinking between CMC, CSN and FU for all the crosslinked hydrogels. Different degrees of semi-crystalline nature, number of peaks, reduction in peak intensities of FU when exposed to the bi-polymer backbones, peak broadening and shifts are observed (Fig. 4b). For example, G1 shows two prominent peaks at $2\theta = 22.15°$ and 35.45° while G3 shows three prominent peaks at $2\theta = 5.66°$, 23.47° and 42.46°. Increase in peak intensities for the crosslinked hydrogel when compared with that of G0 indicates an increase in crystalline nature and material appeal of the developed hydrogels. Shift to higher theta values indicates a decrease in interchain spacing, implying enhanced crosslinking [43]. The XRD patterns are like those published in the literature for the pure polymers [8,39].

Thermograms of CMC, CSN, G0 and G1 (Fig. 5a) indicate intermolecular interaction of the components. Between 25 and 250 °C (Fig. 5a insert), two endothermic peaks are seen for CMC, CSN. The peak becomes broadened for G0, suggesting that it is made from the pure polymers. With an added endothermic peak from FU, G1 shows three endothermic peaks (30 °C, 60–110 °C and 215 °C). All peaks are attributable to heat absorption by water evaporation from the polymers and hydrogels. Also, the heat flow of CMC (−1.44 mW at 286.3 °C) and CSN (−1.55 mW at 300 °C) are reduced for G0 (−19.73 mW at 267 °C), and on further crosslinking with FU, shifts to 278 °C at −19.18 mW for G1. These indicate component interaction, crosslinking degree and reflects the nature of the microstructure of the hydrogels [37]. Thermograms of the hydrogels (Fig. 5b) display corresponding

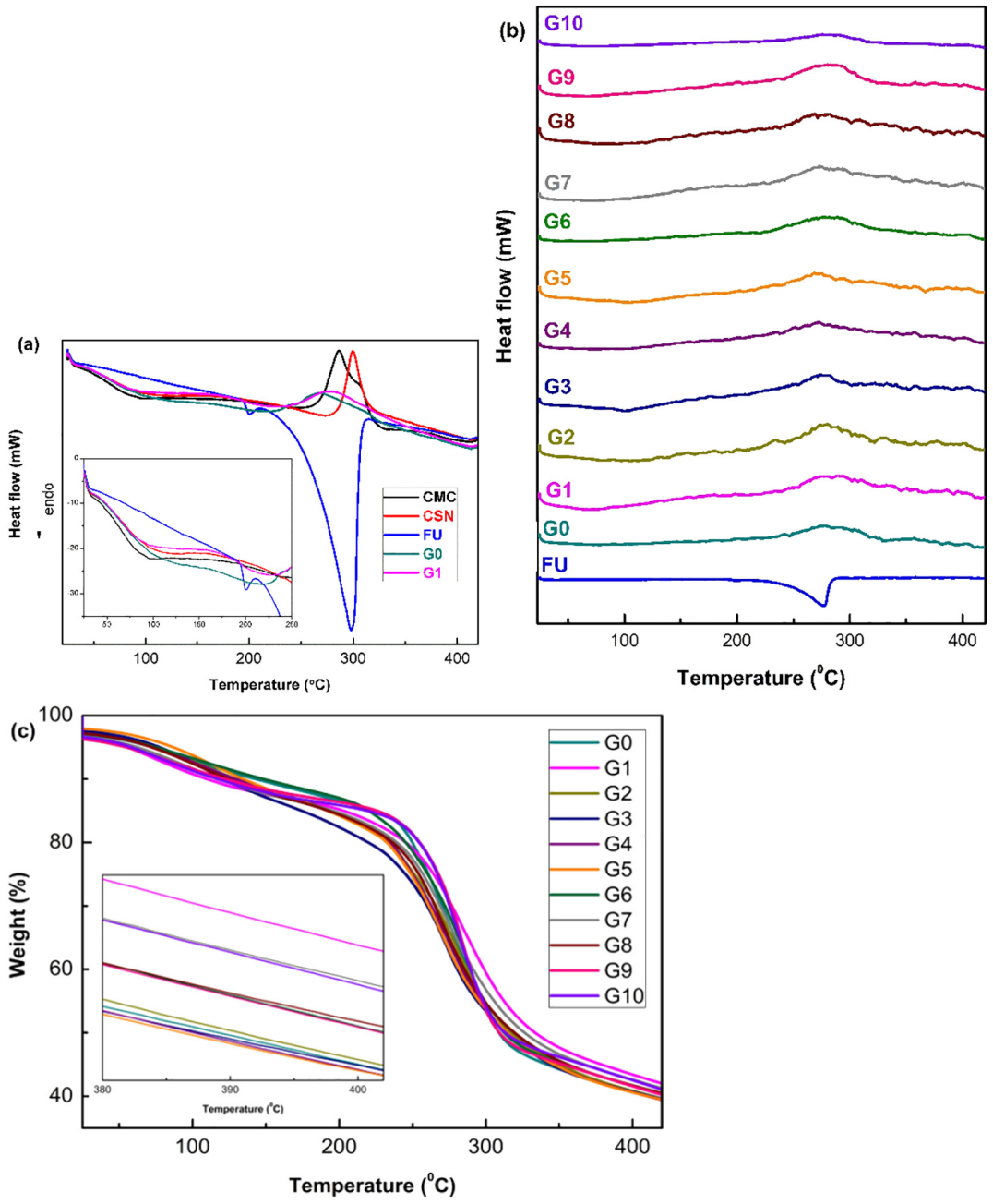


Fig. 5. Thermograms (a) heat flow of G0, FU and hydrogels G1-G10 (inset shows heat flow at 25–250 °C), (b) heat flow of CMC, CSN, G0, and their crosslinking to form G1; and (c) weight (%) of the developed hydrogel.

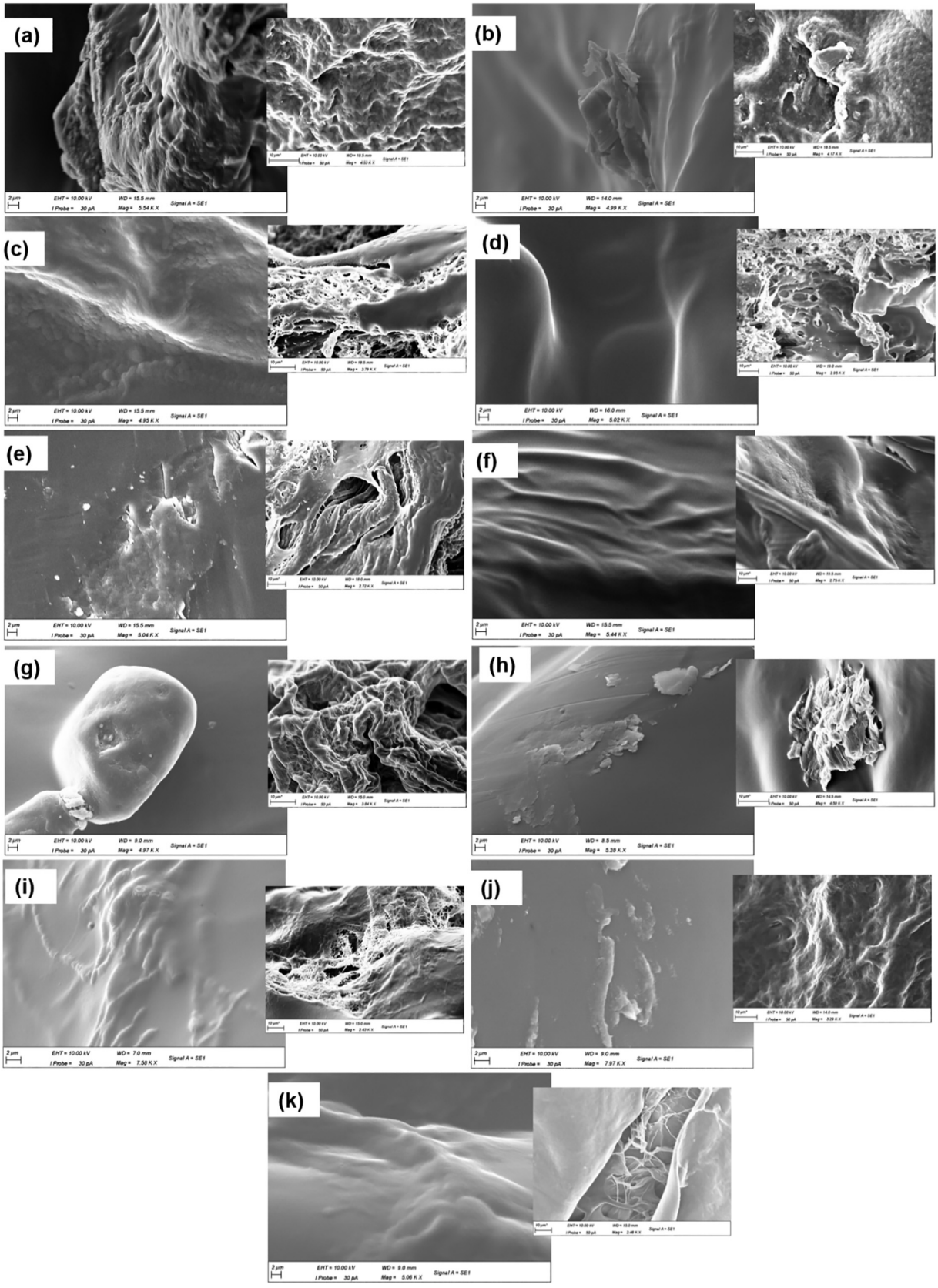


Fig. 6. Micrographs of (a) G0, and developed hydrogels (b) G1, (c) G2, (d) G3, (e) G4, (f) G5, (g) G6, (h) G7, (i) G8, (j) G9, and (k) G10 at dry state. The inserts show micrographs of the hydrogels at swollen state.

peaks like G1 with differences in positions suggesting successful crosslinking between FU and their corresponding CMC and CSN blends. Furthermore, the hydrogels show a similar pattern of three stages mass degradation (Fig. 5c) (25–150 °C, 150–290 °C, and 290–400 °C) due to dehydration of hydrogel free water, vaporization of bound water, and exothermic degradation of polymeric chains, respectively [39]. Cellulose decomposes at 210–260 °C while CSN decomposes starting from 10 °C [44], however, crosslinking suppresses decomposition for the hydrogels to ≈150 °C with about 10% mass loss making them more thermally stable than the pure polymers. Similar results are reported for pure CMC, pure CSN and CMC-CSN [39,44].

3.5. Morphological analysis

Fig. 6 shows surface morphologies of G0 and G1–G10 at dry (2 μm) and swollen (10 μm) (Fig. 6 inserts) states. First, at the dehydrated state, smoothness and uniformity of the surface are indications of good miscibility, homogeneity, and components interaction, hence crosslinking and compactness of microstructure [45]. Without FU (Fig. 6a), G0 shows coarse, non-homogenous surface. With FU, G1–G10 show different degrees of homogenous, smooth, and undulant morphologies. Again, and outstandingly, G3 exhibits the most smooth and homogenous morphology without cracks. This further supports that optimum crosslinking and microstructure is achieved at CMC:CSN = 1:3. Porous networks are not clearly seen at 2 μm. The typical large porous networks seen for most CMC~CSN hydrogels are not reflected in Fig. 6 for the dry samples. This is because lyophilization step/freeze-drying was not included during hydrogel synthesis. The hydrogels were also stored in the desiccator, thoroughly dried, and sealed from air/moisture before the SEM characterization. To make apparent the porous nature, the dry hydrogels were swollen in de-ionized water at 25 °C for 1 h, dried by repeatedly and gently tapping on soft laboratory wipes, and micrographs obtained (Fig. 6 inserts). The hydrogels porous structures become evident (Fig. 6 inserts). Fig. 6 (micrographs at the dry state) is like those reported for polymer-composite hydrogels prepared without a lyophilization step [20,36,46]. The SEM results confirm crosslinking for G1–G10.

3.6. Statistical analysis and model fitting

The effect of variation in polymer ratio on equilibrium swelling ratio and the interaction of the swelling ratio on hydrogel mesh size and a molecular weight between crosslinks were computed. Firstly, the correlation between X1 and X2 and the swelling ratio was evaluated using multiple linear regression, and several models were generated. Fourth order interaction model analysis was used to compute the regression coefficients, and the following final valid statistical polynomial was predicted:

$$\begin{aligned}\hat{y} = {} & 51.5819 - 295.7862X1 + 185.7847X2 \\ & + 230.0731X1^2 - 47.91831X1X2 - 99.66143X2^2 - 62.6301X1^3 \\ & + 5.3289X1^2X2 + 16.4364X1X2^2 + 21.2176X2^3 \\ & + 5.6196X1^4 - 0.6418X1^3X2 - 2.0235X1X2^3 - 1.5209X2^4 \end{aligned} \quad (2)$$

where, the coded variables X1, X2, and $\hat{y}$ represent the CMC ratio, CSN ratio and swelling ratio, respectively. Fig. 7a illustrates the experimental and corresponding predicted values of the swelling ratio for G1–G10. (Data on G1–G19 is given in Table S2, Supplementary information). The developed mathematical model (Eq. (2)) was validated by analyzing statistical parameters (Table S3, Supplementary information) and using a new experimental data set (Fig. 7b). The ANOVA studies (Table S3) show that overall P (1.06×10^{-12}) and the individual P-values of each coefficient which represent the level of significance of the model confirm that the developed model is significant as all are <0.05. Additionally, R^2(0.9876), adjusted R^2 (0.9775) are also close to unity, where (R^2 minus adjusted R^2)/R^2 equals 0.01023. This indicates that when the model is applied to new data set, it could shrink by a small factor of 0.01. Besides, the mean of the residuals (Table S2, Supplementary information) is 0, indicating that the model is systematically unbiased and valid for predictive analysis. Lastly, the model was applied to a new experimental data set at ratios CMC:CSN = 1.5:1(hydrogel H1), 1:1.5(H2), 3.5:1(H3), 1:3:5(H4) and 3.5:2(H5). The swelling ratio (predicted; experimental) results presented (Fig. 7b) show good agreement between the model and the experimental data. Thus, Eq. (2) is statistically valid and is a good predictor of the swelling ratio of the CMC~CSN composite hydrogels within the design space, especially where X1 has less content than X2. Secondly, mathematical model correlations between the variables of mesh size and M_C, and the swelling ratio, x, were evaluated. Fifth degree linear model analysis was used to derive the following polynomial equations:

$$M_C = 0.01192x^5 - 1.837x^4 + 109.3x^3 - 3113x^2 + 42040x - 103400 \quad (3)$$

$$\begin{aligned}\textit{Mesh size} = {} & 0.00003106x^5 - 0.003845x^4 + 0.1818x^3 - 4.13x^2 \\ & + 48.26x - 98.98 \end{aligned} \quad (4)$$

The experimental data presented in Table 1 were verified using Eqs. (3) and (4) (Fig. 7(c–e)). V_C was also estimated using the dry hydrogel density and the predicted M_C values for G1–G19 are given (Table S4, Supplementary information). Fig. 7(c–e) shows good agreement between the predicted and experimental M_C values (Fig. 7c), mesh sizes (Fig. 7d), and the V_C values (Fig. 7e). Thus, using the predicted swelling ratios from Eq. (2), M_C, mesh sizes, and V_C of the hydrogels can also be predicted.

3.7. Analysis of influencing factors - effect of CMC and CSN ratio on swelling

Swelling increases with increasing CMC content but decreases with increasing CSN content. The positive and negative values of the linear and interaction coefficients of the model indicate positive and negative effects on swelling. For example, the p-value of CMC (X1) shows that CMC exerts significant influence on swelling ratio, but the effect is reduced when it interacts with larger CSN content as shown in the p-values of terms, $X1X2^2$ and $X1X2^3$ (Table S3, Supplementary information). Thus, to reduce swelling, promote compact and denser microstructure [8,36], it is recommended that CMC amount be less than that of CSN. Conversely, where super-absorbency is desired, the CMC ratio should be higher.

3.8. Thermal sensitivity and response of G3/PEG and G3/PEG/Bi_2Te_3 coated fabrics

The coated fabrics were subjected to ambient (15 °C), body (33.2 °C) and elevated (45 °C) temperatures and thermal conductivity, resistance and thermal response of the fabrics were examined in comparison with the control sample. At 15 °C and 33.2 °C, the coated fabrics maintain higher thermal conductivity and surface temperature than the uncoated sample (Fig. 8a and b) while at 45 °C, the surface temperature of the coated fabrics drops below (especially G3/PEG/Bi_2Te_3 fabric) that of the uncoated fabric (Fig. 8c). This could be attributed to the presence of all the hydrogel components, especially, PEG. Bi_2Te_3 in G3/PEG/Bi_2Te_3 contributed to the better insulating behavior of the G3/PEG/Bi_2Te_3 coated fabric. At a temperature below its own, the hydrogel coating expands absorbing cool/moist air, maintaining its surface temperature; and at a temperature above its own, shrinks ejecting water molecules (in either gaseous or liquid form) from its matrix, releasing cooling/maintaining its surface temperature. Expansion or shrinkage is due to (1) decreased or increased orderliness of the polymer network and (2) orderliness or disorderliness of water molecules following polymer-polymer and polymer-water interaction [47]. The G3/PEG coated fabric shows enhanced uniform distribution of heat (from body and hotplate) (Fig. 8ci) when compared with the G3/PEG/Bi_2Te_3 coated

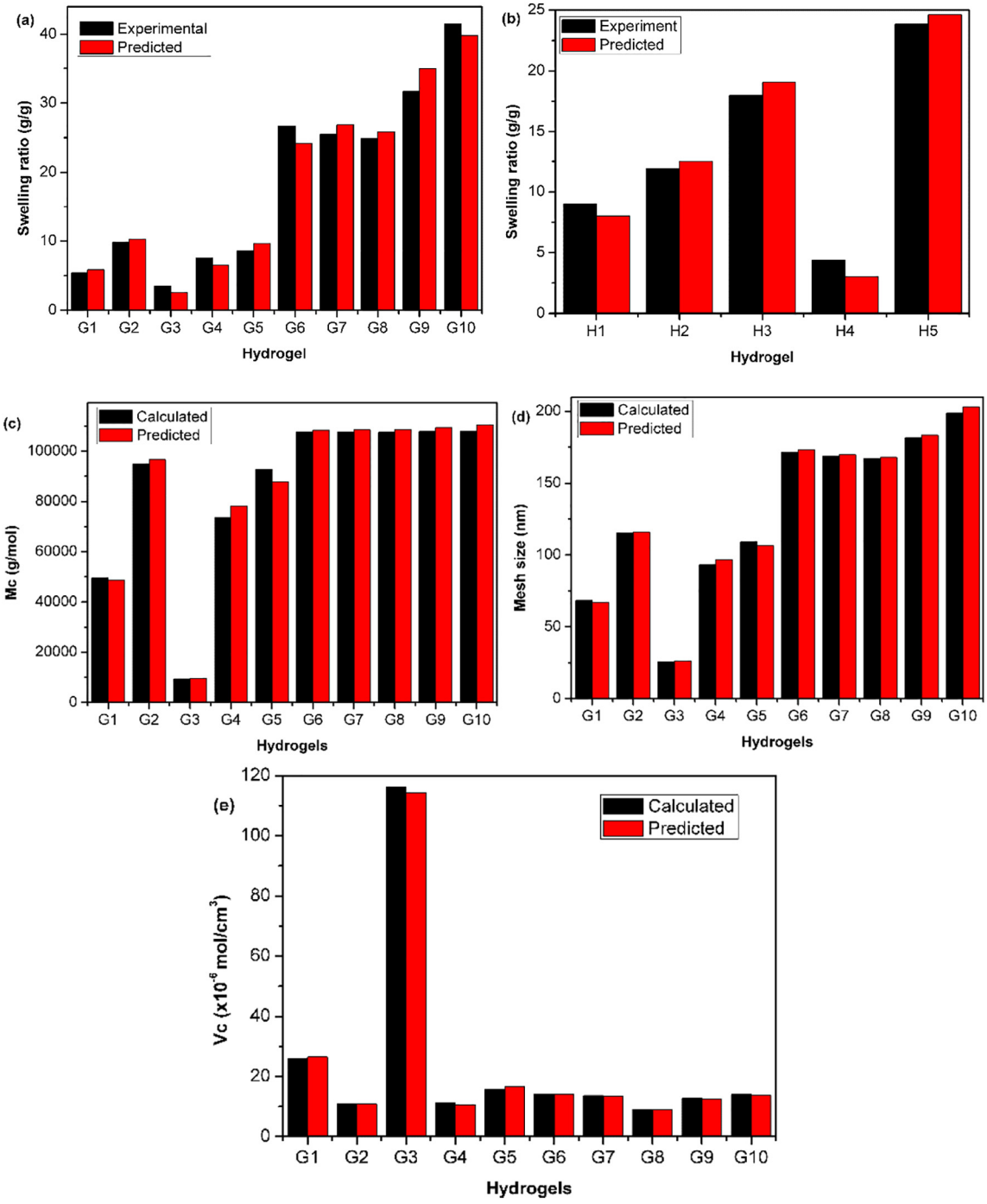


Fig. 7. Hydrogel properties showing experimental and predicted values (a) swelling response of G1-G10, (b) model validation using new data set showing the swelling response of hydrogels H1-H5, and microstructure parameters (c) molecular weight between crosslinks, M_C, (d) mesh size and (e) effective crosslinking density, V_C, of hydrogels G1-G10. Although panel a has $R^2 = 0.9876$, the model exhibits acceptable agreement with the experimental data, thus suitable for predictive studies (panels (b–e)).

fabric (Fig. 8cii). This is because the G3/PEG coated fabric expresses the highest thermal conductivity of all the fabrics (Fig. 8d) while G3/PEG/Bi_2Te_3 coated fabric expresses better insulating characteristic compared with G3/PEG fabric (Fig. 8cii). The thickness (Fig. 8e) of the fabrics could have contributed to the differences in insulation. The calculated CLO values (Fig. 8f) confirm that G3/PEG/Bi_2Te_3 fabric (0.115 ± 0.001 CLO) exhibits higher insulating ability. The thickness, thermal conductivity and thermal resistance results for the uncoated fabric are within the same range as those published [48,49]. These features of G3/PEG and G3/PEG/Bi_2Te_3 can be harnessed for thermoelectric wearable textiles/devices.

4. Conclusion

The influence of the composition of carboxymethyl cellulose and chitosan on swelling and microstructure parameters, such as mesh size, molecular weight between crosslinks (M_C) and effective crosslinking density (V_C) of CMC-CSN composite hydrogel is studied. Mathematical models are generated and validated by analyzing ANOVA parameters and experimental data. The results show that swelling is directly proportional to CMC content but inversely proportional to CSN content and that decreased swelling enhances microstructure compactness. Hydrogel prepared with CMC:CSN = 1:3 exhibits optimum

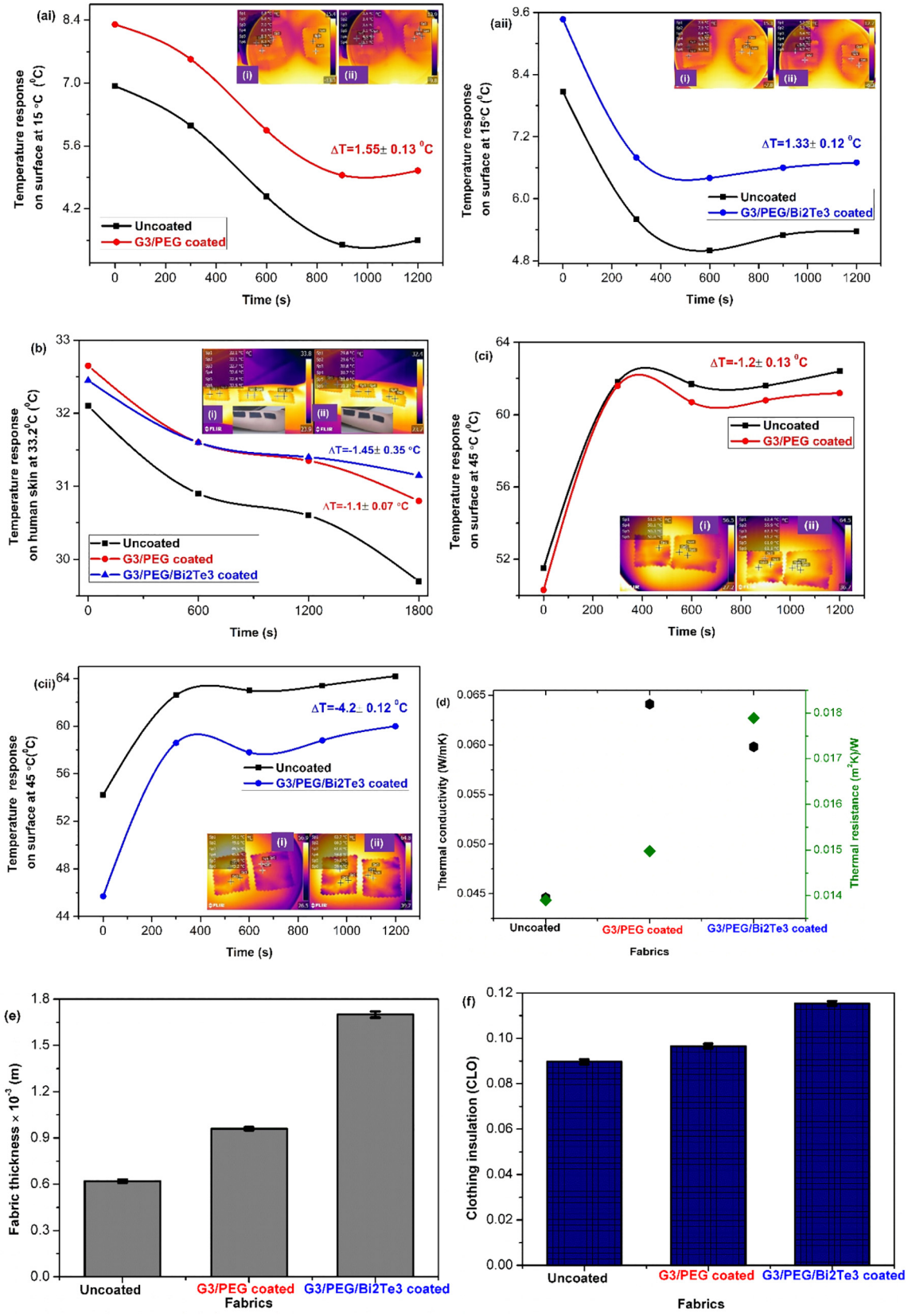


Fig. 8. Fabric temperature-sensitivity (a) at (15 °C) for (ai) uncoated and G3/PEG coated fabrics and (aii) uncoated and G3/PEG/Bi_2Te_3 coated fabrics (the insets show thermal images acquired at (i) 0 min and (ii) after 20 min exposure to 15 °C), (b) on skin at 33.2 °C (inset shows thermal images acquired at (i) 0 min and (ii) after 30 min on skin), (c) at 45 °C for (ci) uncoated and G3/PEG coated fabrics and (cii) uncoated and G3/PEG/Bi_2Te_3 coated fabrics (the inset shows thermal images acquired at (i) 0 min and (ii) after 20 min exposure to 45 °C), (d) thermal conductivity and resistance (e) fabric thickness and (g) clothing insulation values.

microstructure parameters and hydrolytic properties. The ANOVA results of $P = 1.06 \times 10^{-12}$, $R^2 = 0.9876$, and adjusted $R^2 = 0.9775$ and the model agreement with experimental data show that the generated model can be used to characterize hydrogel equilibrium swelling ratio where the ratio of CMC to CSN is known, from which M_C, mesh size, and V_C can be predicted. This study concludes that (1) moderate swelling and optimum microstructure for CMC~FU~CSN hydrogel is achieved at CMC:CSN = 1:3; (2) Eq. (2) can be used to estimate equilibrium swelling; and (3) CMC~FU~CSN is an ideal host matrix for wearable energy applications. This study provides insight into the design of CMC-CSN hydrogels for targeted swelling properties and potential use in the advancement of functional wearable energy textiles.

CRediT authorship contribution statement

Kindness A. Uyanga: Conceptualization, Methodology, Investigation, Formal analysis, Writing- Original draft, Reviewing and Editing. **Walid A. Daoud:** Formal analysis, Validation, Writing- Reviewing and Editing, Funding acquisition, Supervision.

Declaration of competing interest

The authors declare that they have no known competing financial interest or personal relationships that could have influenced this work.

Acknowledgements

The study was funded by the Innovation and Technology Commission of Hong Kong (Grant no. PRP/028/19FX) and City University of Hong Kong (Grant no. 9231255, 9667191, 9239018). The authors thank Mr. Senyi LIU, Ms. Weilu LI, Dr. Lingyun WANG and Dr. Wai Kwok CHUNG for their contributions.

Appendix A. Supplementary data

Supplementary data to this article can be found online at https://doi.org/10.1016/j.ijbiomac.2021.04.117.

References

[1] P. Chen, F. Xie, F. Tang, T. McNally, Glycerol plasticisation of chitosan/carboxymethyl cellulose composites: role of interactions in determining structure and properties, Int. J. Biol. Macromol. 163 (2020) 683–693.
[2] D. Wei, Q. Liu, Z. Liu, J. Liu, X. Zheng, Y. Pei, K. Tang, Modified nano microfibrillated cellulose/carboxymethyl chitosan composite hydrogel with giant network structure and quick gelation formability, Int. J. Biol. Macromol. 135 (2019) 561–568.
[3] P. Chen, F. Xie, F. Tang, T. McNally, Structure and properties of thermomechanically processed chitosan/carboxymethyl cellulose/graphene oxide polyelectrolyte complexed bionanocomposites, Int. J. Biol. Macromol. 158 (2020) 420–429.
[4] J.C. Roy, A. Ferri, S. Giraud, G. Jinping, F. Salauen, Chitosan-carboxymethylcellulose-based polyelectrolyte complexation and microcapsule shell formulation, Int. J. Mol. Sci. 19 (2018) (2521/2521–2521/2519).
[5] M.J. Majcher, T. Hoare, Hydrogel synthesis and design, in: M.A.J. Mazumder, H. Sheardown, A. Al-Ahmed (Eds.) Functional Biopolymers, Springer Nature, Switzerland, 2019.
[6] J.E. Elliott, J.W. Anseth, C.N. Bowman, Kinetic modeling of the effect of solvent concentration on primary cyclization during polymerization of multifunctional monomers, Chem. Eng. Sci. 56 (2001) 3173–3184.
[7] P. Martens, A.T. Metters, K.S. Anseth, C.N. Bowman, A generalized bulk-degradation model for hydrogel networks formed from multivinyl cross-linking molecules, J. Phys. Chem. B 105 (2001) 5131–5138.
[8] K.A. Uyanga, O.P. Okpozo, O.S. Onyekwere, W.A. Daoud, Citric acid crosslinked natural bi-polymer-based composite hydrogels: effect of polymer ratio and beta-cyclodextrin on hydrogel microstructure, React. Funct. Polym. 154 (2020), 104682, .
[9] J. Shang, Z. Shao, X. Chen, Electrical behavior of a natural polyelectrolyte hydrogel: chitosan/Carboxymethylcellulose hydrogel, Biomacromolecules 9 (2008) 1208–1213.
[10] L. Bao, X. Chen, B. Yang, Y. Tao, Y. Kong, Construction of electrochemical chiral interfaces with integrated polysaccharides via Amidation, ACS Appl. Mater. Interfaces 8 (2016) 21710–21720.
[11] H.G. Kim, L.K. Kwac, Y.-S. Kim, H.K. Shin, K.-Y. Rhee, Synthesis and characterization of eco-friendly carboxymethyl cellulose based carbon foam using electron beam irradiation, Compos. Part B-Eng 151 (2018) 154–160.
[12] A.F. Martins, J. Vlcek, T. Wigmosta, M. Hedayati, M.M. Reynolds, K.C. Popat, M.J. Kipper, Chitosan/iota-carrageenan and chitosan/pectin polyelectrolyte multilayer scaffolds with antiadhesive and bactericidal properties, Appl. Surf. Sci. 502 (2020) 144282.
[13] V. Dinca, P. Alloncle, P. Delaporte, V. Ion, L. Rusen, M. Filipescu, C. Mustaciosu, C. Luculescu, M. Dinescu, Excimer laser texturing of natural composite polymer surfaces for studying cell-to-substrate specific response, Appl. Surf. Sci. 352 (2015) 82–90.
[14] S. Kaihara, Y. Suzuki, K. Fujimoto, In situ synthesis of polysaccharide nanoparticles via polyion complex of carboxymethyl cellulose and chitosan, Colloids Surf. B 85 (2011) 343–348.
[15] Z. Zhang, J. Tan, W. Gu, H. Zhao, J. Zheng, B. Zhang, G. Ji, Cellulose-chitosan framework/polyailine hybrid aerogel toward thermal insulation and microwave absorbing application, Chem. Eng. J. 395 (2020), 125190, .
[16] K. Manzoor, M. Ahmad, S. Ahmad, S. Ikram, Removal of Pb(II) and cd(II) from wastewater using arginine cross-linked chitosan-carboxymethyl cellulose beads as green adsorbent, RSC Adv. 9 (2019) 7890–7902.
[17] M. Ahuja Minkal, D.C. Bhatt, Polyelectrolyte complex of carboxymethyl gum katira-chitosan: preparation and characterization, Int. J. Biol. Macromol. 106 (2018) 1184–1191.
[18] G.M. Asnag, A.H. Oraby, A.M. Abdelghany, Green synthesis of gold nanoparticles and its effect on the optical, thermal and electrical properties of carboxymethyl cellulose, Compos. Part B-Eng 172 (2019) 436–446.
[19] L. Wang, X. Yang, W.A. Daoud, High power-output mechanical energy harvester based on flexible and transparent au nanoparticle-embedded polymer matrix, Nano Energy 55 (2019) 433–440.
[20] E. Akar, A. Altınışık, Y. Seki, Preparation of pH- and ionic-strength responsive biodegradable fumaric acid crosslinked carboxymethyl cellulose, Carbohydr. Polym. 90 (2012) 1634–1641.
[21] R.-A. Ilica, L. Kloetzer, A.-I. Galaction, D. Caşcaval, Fumaric acid: production and separation, Biotechnol. Lett. (2018) 1–11.
[22] L. He, H. Wang, H. Zhu, Y. Gu, X. Li, X. Mao, Thermal properties of PEG/graphene Nanoplatelets (GNPs) composite phase change materials with enhanced thermal conductivity and photo-thermal performance, Appl. Sci. 8 (2018) 2613.
[23] P. Yuan, P. Zhang, T. Liang, S. Zhai, Effects of surface functionalization on thermal and mechanical properties of graphene/polyethylene glycol composite phase change materials, Appl. Surf. Sci. 485 (2019) 402–412.
[24] M. Zhang, H. Mao, Z. Jin, Molecular dynamic study on structural and dynamic properties of water, counter-ions and polyethylene glycols in Na-montmorillonite interlayers, Appl. Surf. Sci. 536 (2021), 147700, .
[25] T. Wang, Y. Qi, J. Xu, X. Hu, P. Chen, Effects of poly(ethylene glycol) on electrical conductivity of poly(3,4-ethylenedioxythiophene)–poly(styrenesulfonic acid) film, Appl. Surf. Sci. 250 (2005) 188–194.
[26] N.S.V. Capanema, A.A.P. Mansur, A.C. de Jesus, S.M. Carvalho, L.C. de Oliveira, H.S. Mansur, Superabsorbent crosslinked carboxymethyl cellulose-PEG hydrogels for potential wound dressing applications, Int. J. Biol. Macromol. 106 (2018) 17.
[27] M. Saleemi, M.S. Toprak, S. Li, M. Johnsson, M. Muhammed, Synthesis, processing, and thermoelectric properties of bulk nanostructured bismuth telluride ($B_{i2}Te_3$), J. Mater. Chem. 22 (2012) 725–730.
[28] Z. Zeng, P. Yang, Z. Hu, Temperature and size effects on electrical properties and thermoelectric power of bismuth telluride thin films deposited by co-sputtering, Appl. Surf. Sci. 268 (2013) 472–476.
[29] K. Ahmad, C. Wan, M.A. Al-Eshaikh, A.N. Kadachi, Enhanced thermoelectric performance of $B_{i2}Te_3$ based graphene nanocomposites, Appl. Surf. Sci. 474 (2019) 2–8.
[30] Y. Du, J. Xu, B. Paul, P. Eklund, Flexible thermoelectric materials and devices, Appl. Mater. Today 12 (2018) 366–388.
[31] Y.M. Cho, K.T. Kim, G.S. Lee, S.H. Kim, The role of edge-oxidized graphene to improve the thermopower of p-type bismuth telluride-based thick films, Appl. Surf. Sci. 476 (2019) 533–538.
[32] K. Uyanga, P. Onaji, M.O. Okwu, Development of erasable whiteboard marker inks, Can. Int. J. Sci. Technol. (2017) 64–94.
[33] C.P. Gomes, R.C.S. Dias, M.R.P.F.N. Costa, Polymer reaction engineering tools to tailor smart and superabsorbent hydrogels, Cellulose-Based Superabsorb. Hydrogel (2018) 1–63.
[34] X. Feng, R. Pelton, Carboxymethyl cellulose: polyvinylamine complex hydrogel swelling, Macromolecules 40 (2007) 6.
[35] G.O. Akalin, M. Pulat, Preparation and characterization of nanoporous sodium carboxymethyl cellulose hydrogel beads, J. Nanomater. 2018 (2018) 1–12.
[36] Y. Seki, A. Altinisik, B. Demircioğlu, C. Tetik, Carboxymethylcellulose (CMC)-hydroxyethylcellulose (HEC) based hydrogels: synthesis and characterization, Cellulose 21 (2014) 1689–1698.
[37] K. Wang, L. Du, C. Zhang, Z. Lu, F. Lu, H. Zhao, Preparation of chitosan/curdlan/carboxymethyl cellulose blended film and its characterization, J. Food Sci. Technol. 56 (2019) 5396–5404.
[38] X. Zhu, L. Bao, Y. Wei, J. Ma, Y. Kong, Removal of toxic indigo blue with integrated biomaterials of sodium carboxymethyl cellulose and chitosan, Int. J. Biol. Macromol. 91 (2016) 409–415.
[39] S. Benghanem, A. Chetouani, M. Elkolli, M. Bounekhel, D. Benachour, Grafting of oxidized carboxymethyl cellulose with hydrogen peroxide in presence of Cu(II) to chitosan and biological elucidation, Biocybern. Biomed. Eng. 37 (2017) 94–102.
[40] G. Priya, U. Narendrakumar, I. Manjubala, Thermal behavior of carboxymethyl cellulose in the presence of polycarboxylic acid crosslinkers, J. Therm. Anal. Calorim. 138 (2019) 89–95.
[41] H.E. Salama, M.S. Abdel Aziz, M.W. Sabaa, Development of antibacterial carboxymethyl cellulose/chitosan biguanidine hydrochloride edible films activated with frankincense essential oil, Int. J. Biol. Macromol. 139 (2019) 1162–1167.

[42] Y. Jampafuang, A. Tongta, Y. Waiprib, Impact of crystalline structural differences between alpha- and beta-chitosan on their nanoparticle formation via ionic gelation and superoxide radical scavenging activities, Polymers 11 (2019) 2010.
[43] M.K. Jaiswal, J.R. Xavier, J.K. Carrow, P. Desai, D. Alge, A.K. Gaharwar, Mechanically stiff nanocomposite hydrogels at ultralow nanoparticle content, ACS Nano 10 (2016) 246–256.
[44] K. Manzoor, M. Ahmad, S. Ahmad, S. Ikram, Synthesis, characterization, kinetics, and thermodynamics of EDTA-modified chitosan-carboxymethyl cellulose as cu(II) Ion adsorbent, ACS Omega 4 (2019) 17425–17437.
[45] C.N. Grover, J.H. Gwynne, N. Pugh, S. Hamaia, R.W. Farndale, S.M. Best, R.E. Cameron, Crosslinking and composition influence the surface properties, mechanical stiffness and cell reactivity of collagen-based films, Acta Biomater. 8 (2012) 3080–3090.
[46] T.S. Franco, R.M.J. Amezcua, A.V. Rodriguez, S.G. Enriquez, M.R. Urquiza, E.M. Mijares, G.B. de Muniz, Carboxymethyl and nanofibrillated cellulose as additives on the preparation of chitosan biocomposites: their influence over films characteristics, J. Polym. Environ. 28 (2020) 676–688.
[47] M.A. Ward, T.K. Georgiou, Thermoresponsive polymers for biomedical applications, Polymers 3 (2011) 1215–1242.
[48] A. Majumdar, S. Mukhopadhyay, R. Yadav, Thermal properties of knitted fabrics made from cotton and regenerated bamboo cellulosic fibres, Int. J. Therm. Sci. 49 (2010) 2042–2048.
[49] N. Oğlakcioğlu, A. Marmarali, Thermal comfort properties of some knitted structures, Fibre Text East Eur. 15 (2007) 2.